Hypersonic Three-Dimensional Viscous Shock-Layer Flows over Blunt Bodies

Alvin L. Murray* and Clark H. Lewis†
Virginia Polytechnic Institute and State University, Blacksburg, Va.

The viscous shock-layer equations have been extended to treat blunt three-dimensional bodies at angle of attack. Numerical solutions have been obtained on sphere-cones at angles of attack up to 38 deg. Comparisons are made with available experimental data, inviscid solutions, and solutions of the parabolized Navier-Stokes equations. The experimental data consisted of heat-transfer distributions, pressure distributions, and drag coefficients in a Mach number range from 10-18, Reynolds numbers of the order 1.3×10^4/ft, and α from 0-40 deg. Two cases were compared with the parabolized Navier-Stokes solutions at Mach numbers of 22.77 and 25.81 and altitudes of 180 and 240 kft at angles of attack of 23 and 38 deg, respectively. In general, the shock-layer predictions were in good agreement with the available experimental and numerical data, but the parabolic treatment of the crossflow viscous shock-layer equations prevented solutions on the leeward side of long bodies at large angles of attack.

Nomenclature

a = speed of sound
A_i = coefficients of a parabolic differential equation
c_p = specific heat at constant pressure
C' = variable in Sutherland viscosity law
C_D = drag coefficient, 2 drag/$A_{\text{ref}}\rho_\infty U_\infty^2$
C_{f_ξ} = streamwise friction coefficient, $2\tau_\xi^*/\rho_\infty U_\infty^2$
C_{f_ϕ} = transverse friction coefficient, $2\tau_\phi^*/\rho_\infty U_\infty^2$
C_{h_∞} = heat-transfer coefficient, $-q^*/\rho_\infty U_\infty c_p^*(T_{aw}^*-T_w^*)$
C_p = pressure coefficient, $2(p_w^*-p_\infty)/\rho_\infty U_\infty^2$
h = static enthalpy, h^*/U_∞^2
h_1 = shape factor in the streamwise direction, $h_1=1+\kappa_s n_{sh}\eta\cos\theta_s$
h_3 = shape factor in the crossflow direction, $h_3=r(1+\kappa_\phi\eta\cos\theta_s)/\cos\theta_\phi$
H = stagnation enthalpy, H^*/U_∞^2
i = step counter in the streamwise direction
j = step counter in the normal direction
k = step counter in the cross flow direction
m_1, m_2 = integrals used in solution of continuity equation
m = mass of one gas molecule
M = Mach number
n = normal distance from body surface, n^*/R_n^*
N = number density of gas molecules, number of molecules/vol
p = pressure, $p^*/\rho_\infty U_\infty^2$
Pr = Prandtl number
q = heat-transfer rate, $q^*/\rho_\infty U_\infty^3$
r = distance from and normal to body axis, r^*/R_n^*
R = gas constant
R_n^* = nose radius
St_∞ = Stanton number, $-q^*/\rho_\infty U_\infty(H_0^*-H_w^*)$
T = temperature, T^*/T_{ref}^*
T_{ref} = reference temperature, U_∞^2/c_p^* or $(\gamma-1)M_\infty^2 T_\infty$
u = tangential velocity in the streamwise direction, u^*/U_∞
v = normal velocity, v^*/U_∞
v' = transformed normal velocity, $v/(RT)^{1/2}$
v_w' = transformed normal velocity at the wall, $v_w/(RT_w)^{1/2}$
w = tangential velocity in the crossflow direction, w^*/U_∞
W = general dependent variable
X_3 = h_3/r
α = angle of attack, deg
α_t = thermal accommodation coefficient
β = wall porosity, open area divided by solid area
γ = ratio of specific heats
ϵ = Reynolds number parameter, $\epsilon^2=\mu^*(T_{\text{ref}}^*)/\rho_\infty U_\infty R_n^*$
ζ,ϕ = transverse coordinate in the coordinate system (ξ,η,ζ)
η = normalized coordinate in the direction normal to the body surface, n/n_{sh}
θ_s = body angle in the streamwise direction (see Fig. 1)
θ_t = parameter proportional to the number of diffusely reflected molecules
θ_ϕ = body angle between the radius vector and the line tangent to the body surface in the plane ζ = const (see Fig. 1)
κ_s = body curvature in the ξ direction
κ_ϕ = body curvature in the ζ direction
μ = viscosity, $\mu^*/\mu^*(T_{\text{ref}}^*)$
ξ,s = streamwise coordinate in the system (ξ,η,ζ)
ρ = density, ρ^*/ρ_∞
σ = angle between the freestream velocity vector and the vector tangent to the shock surface in the plane formed by the shock-normal vector
τ = shear-stress component

Superscripts

$\bar{(\ )}$ = variable which has been normalized by the value behind the bow shock wave
$*$ = dimensional quantity
$\hat{(\ )}$ = denotes shock normal coordinate system

Subscripts

aw = adiabatic wall conditions
I = conditions in the injection chamber
s = streamwise direction
sh = conditions behind the bow shock wave

Presented as Paper 78-259 at the AIAA 16th Aerospace Sciences Meeting, Huntsville, Ala., Jan. 16-18, 1978; submitted Feb. 28, 1978; revision received Aug. 2, 1978.

Index categories: Supersonic and Hypersonic Flow; Viscous Nonboundary-Layer Flows.

*Research Associate, Aerospace and Ocean Engineering Dept.; presently at Acurex Corporation, Mountain View, Calif. Student Member AIAA.

†Professor, Aerospace and Ocean Engineering Dept. Associate Fellow AIAA.

w = wall condition
0 = stagnation point conditions
ζ = derivative with respect to ζ
ϕ = transverse direction
∞ = dimensional freestream quantity

Introduction

In recent years, the two-dimensional viscous shock-layer equations have been applied to a wide range of problems by a number of investigators.[1-6] The shock-layer approach is receiving more attention because of the advantages it offers. The classical approach to solving a flowfield problem is to divide the flow into an inviscid outer region and a viscous boundary-layer region. The wall values of the inviscid solution are used as edge conditions for the viscous solution. This approach works well at high Reynolds numbers where the viscous region is very thin. At low Reynolds numbers, the viscous region is thick, and the displacement effect must be modeled by interacting the viscous calculation with the inviscid solution. Another problem with this approach is determining the edge conditions for the boundary-layer calculation. Methods such as streamline tracking and entropy-layer swallowing have been used to help solve this problem. The viscous shock-layer equations treat the entire flowfield uniformly and have no problem with displacement effects. The edge conditions for the shock-layer approach are obtained easily from the Rankine-Hugoniot equations. Another advantage of the shock-layer approach is the equations are parabolic and may be solved easily. Solutions of the full Navier-Stokes equations are complex and time consuming because of the elliptic nature of the equations. Even the parabolized Navier-Stokes method of Lubard and Helliwell[7] is elliptic in the crossflow direction and requires iterative solutions of the governing equations.

The purpose of the present work is to develop a procedure which may be used as a tool in the analysis and design of re-entry vehicles. The method must be efficient and give reasonably accurate predictions of wall-measurable quantities as well as flowfield solutions on bodies at high altitudes and large angles of attack. The viscous shock-layer approach originally developed by Davis[1] for axisymmetric or two-dimensional bodies at zero lift has given good predictions in low Reynolds number flows similar to those encountered during re-entry. At high altitudes or low densities, the effects of wall slip and temperature jump and shock slip are significant and can be incorporated easily into the shock-layer technique. The procedure has been shown to be both efficient and accurate for axisymmetric flows but has not been extended to complete three-dimensional flowfields. Since the governing equations are also parabolic in the crossflow direction, the method will not be able to treat leeside flows beyond crossflow separation. At high angles of attack, the pressures on the leeside are small when compared to the windward side and should not make a significant contribution to the aerodynamic forces.

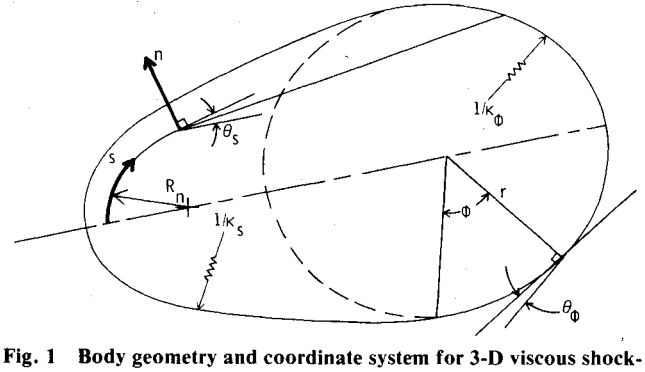

Fig. 1 Body geometry and coordinate system for 3-D viscous shock-layer predictions.

The three-dimensional shock-layer equations are presented with both longitudinal and transverse curvature terms included. The boundary conditions used include slip at both the body and bow shock wave and wall mass transfer. The procedure has been applied to sphere-cones at large angles of attack and comparisons made with experimental data in an effort to validate the method.

Analysis

The viscous shock-layer equations are derived from the Navier-Stokes equations. The conservation equations are first nondimensionalized by variables which are of order one in the region near the body surface and in the inviscid region. The normal velocity v and normal coordinate n are assumed to be of order ϵ and terms which are second order are retained in the s momentum, ϕ momentum, and energy equations. The equations are then normalized by the local shock values of the variables to aid in the solution procedure.

A spherically blunted cone is a typical re-entry vehicle. The equations are developed in an orthogonal coordinate system (ξ,η,ζ) where the ξ coordinate is tangent to the body in the streamwise direction, η is the coordinate normal to the surface, and the ϕ coordinate is the angle around the body measured from the windward streamline (see Fig. 1). Both longitudinal and transverse curvature are included in the development of the equations which is given in detail by Murray and Lewis.[8]

Governing Equations

The equations may be written in the form

$$A_0\frac{\partial^2 W}{\partial\eta^2}+A_1\frac{\partial W}{\partial\eta}+A_2W+A_3+A_4\frac{\partial W}{\partial\xi}+A_5\frac{\partial W}{\partial\zeta}=0$$

where W is the dependent variable. The coefficients for the equations are:

ξ Momentum:

$$A_0=-\frac{\epsilon^2\mu_{sh}\bar{\mu}}{n_{sh}^2}$$

$$A_1=-\frac{\epsilon^2\mu_{sh}}{n_{sh}^2}\frac{\partial\bar{\mu}}{\partial\eta}+\frac{\epsilon^2\mu_{sh}\bar{\mu}}{n_{sh}^2h_1}\frac{\partial h_1}{\partial\eta}-\frac{\rho_{sh}u_{sh}\eta}{h_1n_{sh}}\frac{\partial n_{sh}}{\partial\xi}\bar{\rho}\bar{\mu}$$
$$+\frac{\rho_{sh}\bar{\rho}v}{n_{sh}}-\frac{\rho_{sh}\eta\bar{\rho}w}{h_3n_{sh}}\frac{\partial n_{sh}}{\partial\zeta}-\frac{\epsilon^2\mu_{sh}\bar{\mu}}{n_{sh}^2}\left(\frac{2}{h_1}\frac{\partial h_1}{\partial\eta}+\frac{1}{h_3}\frac{\partial h_3}{\partial\eta}\right)$$

$$A_2=\frac{\rho_{sh}\bar{\rho}\bar{\mu}}{h_1}\frac{\partial u_{sh}}{\partial\xi}+\frac{\rho_{sh}\bar{\rho}w}{h_3u_{sh}}\frac{\partial u_{sh}}{\partial\zeta}+\frac{\rho_{sh}\bar{\rho}v}{h_1n_{sh}}\frac{\partial h_1}{\partial\eta}$$
$$+\frac{\rho_{sh}\bar{\rho}w}{h_1h_3}\frac{\partial h_1}{\partial\zeta}-\frac{\rho_{sh}\bar{\rho}w\eta}{h_1h_3n_{sh}}\frac{\partial n_{sh}}{\partial\zeta}\frac{\partial h_1}{\partial\eta}+\frac{\epsilon^2\mu_{sh}}{n_{sh}^2}\frac{\partial}{\partial\eta}\left(\frac{\mu}{h_1}\frac{\partial h_1}{\partial\eta}\right)$$
$$+\frac{\epsilon^2\mu_{sh}\bar{\mu}}{n_{sh}^2h_1}\left(\frac{2}{h_1}\frac{\partial h_1}{\partial\eta}+\frac{1}{h_3}\frac{\partial h_3}{\partial\eta}\right)\frac{\partial h_1}{\partial\eta}$$

$$A_3=-\frac{\rho_{sh}\bar{\rho}w^2}{h_1h_3u_{sh}}\frac{\partial h_3}{\partial\xi}+\frac{\rho_{sh}\eta\bar{\rho}w^2}{h_1h_3n_{sh}u_{sh}}\frac{\partial n_{sh}}{\partial\xi}\frac{\partial h_3}{\partial\eta}+\frac{\bar{p}}{h_1u_{sh}}\frac{\partial p_{sh}}{\partial\xi}$$
$$+\frac{p_{sh}}{h_1u_{sh}}\frac{\partial\bar{p}}{\partial\xi}-\frac{p_{sh}\eta}{h_1n_{sh}u_{sh}}\frac{\partial n_{sh}}{\partial\xi}\frac{\partial\bar{p}}{\partial\eta}$$

$$A_4=\frac{\rho_{sh}u_{sh}\bar{\rho}\bar{u}}{h_1}$$

$$A_5=\frac{\rho_{sh}\bar{\rho}w}{h_3}$$

ζ Momentum (crossflow):

$$A_0 = -\frac{\epsilon^2 \mu_{sh} \bar{\mu}}{n_{sh}^2}$$

$$A_1 = -\frac{\rho_{sh} u_{sh} \bar{\rho} \bar{u}}{h_1 n_{sh}} \frac{\partial n_{sh}}{\partial \xi} + \frac{\rho_{sh} \bar{\rho} v}{n_{sh}} - \frac{\rho_{sh} \eta \bar{\rho} w}{h_3 n_{sh}} \frac{\partial n_{sh}}{\partial \zeta}$$
$$- \frac{\epsilon^2 \mu_{sh}}{n_{sh}^2} \frac{\partial \bar{\mu}}{\partial \eta} - \frac{\epsilon^2 \mu_{sh} \bar{\mu}}{n_{sh}^2 h_3} \frac{\partial h_3}{\partial \eta} - \frac{\epsilon^2 \mu_{sh} \bar{\mu}}{h_1 n_{sh}^2} \frac{\partial h_1}{\partial \eta}$$

$$A_2 = \frac{\rho_{sh} u_{sh} \bar{\rho} \bar{u}}{h_1 h_3} \frac{\partial h_3}{\partial \xi} - \frac{\rho_{sh} u_{sh} \bar{\rho} \bar{u}}{h_1 h_3 n_{sh}} \frac{\partial n_{sh}}{\partial \xi} \frac{\partial h_3}{\partial \eta} \eta$$
$$+ \frac{\rho_{sh} \bar{\rho} v}{h_3 n_{sh}} \frac{\partial h_3}{\partial \eta} + \frac{\epsilon^2 \mu_{sh} \bar{\mu}}{h_3 n_{sh}^2} \frac{\partial^2 h_3}{\partial \eta^2} + \frac{\epsilon^2 \mu_{sh} \bar{\mu}}{n_{sh}^2 h_3^2} \left(\frac{\partial h_3}{\partial \eta} \right)^2$$
$$+ \frac{\epsilon^2 \mu_{sh}}{n_{sh}^2 h_3} \frac{\partial \bar{\mu}}{\partial \eta} \frac{\partial h_3}{\partial \eta} + \frac{\epsilon^2 \mu_{sh} \bar{\mu}}{h_1 h_3 n_{sh}^2} \frac{\partial h_1}{\partial \eta} \frac{\partial h_3}{\partial \eta}$$

$$A_3 = -\frac{\rho_{sh} u_{sh}^2 \bar{\rho} \bar{u}^2}{h_1 h_3} \frac{\partial h_1}{\partial \zeta} + \frac{\rho_{sh} u_{sh}^2 \bar{\rho} \bar{u}^2 \eta}{h_1 h_3 n_{sh}} \frac{\partial n_{sh}}{\partial \zeta} \frac{\partial h_1}{\partial \eta}$$
$$+ \frac{p_{sh}}{h_3} \frac{\partial \bar{p}}{\partial \zeta} + \frac{\bar{p}}{h_3} \frac{\partial p_{sh}}{\partial \zeta} - \frac{p_{sh} \eta}{h_3 n_{sh}} \frac{\partial n_{sh}}{\partial \zeta} \frac{\partial \bar{p}}{\partial \eta}$$

$$A_4 = \frac{\rho_{sh} u_{sh} \bar{\rho} \bar{u}}{h_1}$$

$$A_5 = \frac{\rho_{sh} \bar{\rho} w}{h_3}$$

Energy:

$$A_0 = -\frac{\epsilon^2 \mu_{sh} \bar{\mu} h_{sh}}{n_{sh}^2 Pr}$$

$$A_1 = -\frac{\epsilon^2 \mu_{sh} h_{sh}}{n_{sh}^2 Pr} \frac{\partial \bar{\mu}}{\partial \eta} - \frac{\epsilon^2 \mu_{sh} h_{sh} \bar{\mu}}{n_{sh}^2 h_1 Pr} \frac{\partial h_1}{\partial \eta} - \frac{\epsilon^2 \mu_{sh} h_{sh} \bar{\mu}}{n_{sh}^2 h_3 Pr} \frac{\partial h_3}{\partial \eta}$$
$$+ \frac{\rho_{sh} h_{sh} \bar{\rho} v}{n_{sh}} - \frac{\rho_{sh} h_{sh} \bar{\rho} w \eta}{h_3 n_{sh}} \frac{\partial n_{sh}}{\partial \zeta} - \frac{\rho_{sh} u_{sh} h_{sh} \bar{\rho} \bar{u} \eta}{h_1 n_{sh}} \frac{\partial n_{sh}}{\partial \xi}$$

$$A_2 = \frac{\rho_{sh} u_{sh} \bar{\rho} \bar{u}}{h_1} \frac{\partial h_{sh}}{\partial \xi} + \frac{\rho_{sh} \bar{\rho} w}{h_3} \frac{\partial h_{sh}}{\partial \zeta}$$

$$A_3 = -\frac{p_{sh} u_{sh} \bar{u}}{h_1} \frac{\partial \bar{p}}{\partial \xi} - \frac{u_{sh} \bar{\rho} \bar{u}}{h_1} \frac{\partial p_{sh}}{\partial \xi} + \frac{p_{sh} u_{sh} \bar{u} \eta}{h_1 n_{sh}} \frac{\partial n_{sh}}{\partial \xi} \frac{\partial \bar{p}}{\partial \eta}$$
$$- \frac{p_{sh} v}{n_{sh}} \frac{\partial p}{\partial \eta} - \frac{p_{sh} w}{h_3} \frac{\partial \bar{p}}{\partial \zeta} - \frac{\bar{p} w}{h_3} \frac{\partial p_{sh}}{\partial \zeta} + \frac{p_{sh} w \eta}{h_3 n_{sh}} \frac{\partial n_{sh}}{\partial \zeta} \frac{\partial \bar{p}}{\partial \eta}$$
$$- \epsilon^2 \mu_{sh} \bar{\mu} \left(\frac{u_{sh}}{n_{sh}} \frac{\partial \bar{u}}{\partial \eta} - \frac{u_{sh} \bar{u}}{h_1 n_{sh}} \frac{\partial h_1}{\partial \eta} \right)^2$$
$$- \epsilon^2 \mu_{sh} \bar{\mu} \left(\frac{1}{n_{sh}} \frac{\partial w}{\partial \eta} - \frac{w}{h_3 n_{sh}} \frac{\partial h_3}{\partial \eta} \right)^2$$

$$A_4 = \frac{\rho_{sh} u_{sh} \bar{\rho} \bar{u} h_{sh}}{h_1}$$

$$A_5 = \frac{\rho_{sh} \bar{\rho} w h_{sh}}{h_3}$$

Note that the normal velocity v and crossflow velocity w are not normalized by the values behind the bow shock. Non-dimensional rather than normalized v and w are used to eliminate problems which occur when the normalized variables become indeterminate. At the stagnation point, the shock value of v is negative, whereas downstream on a slender body v_{sh} becomes positive and thus there exists a point where $v_{sh} = 0$. A similar problem occurs on the windward and leeward planes where $w_{sh} = 0$. These indeterminate quantities, if used in the solution algorithm, would destroy the accuracy of the solution.

The continuity and normal momentum equations remain first order and are given by

Continuity:

$$\frac{\partial}{\partial \xi} (\rho_{sh} u_{sh} \bar{\rho} \bar{u} h_3) - \frac{\eta}{n_{sh}} \frac{\partial n_{sh}}{\partial \xi} \frac{\partial}{\partial \eta} (\rho_{sh} u_{sh} \bar{\rho} \bar{u} h_3)$$
$$+ \frac{1}{n_{sh}} \frac{\partial}{\partial \eta} (h_1 h_3 \rho_{sh} \bar{\rho} v) + \frac{\partial}{\partial \zeta} (h_1 \rho_{sh} \bar{\rho} w)$$
$$- \frac{\eta}{n_{sh}} \frac{\partial n_{sh}}{\partial \zeta} \frac{\partial}{\partial \eta} (\rho_{sh} \bar{\rho} w h_1) = 0$$

Normal Momentum:

$$\frac{\partial \bar{p}}{\partial \eta} = -\frac{\rho_{sh} u_{sh} n_{sh} \bar{\rho} \bar{u}}{p_{sh} h_1} \frac{\partial v}{\partial \xi} - \frac{\rho_{sh} n_{sh} \bar{\rho} w}{p_{sh} h_3} \frac{\partial v}{\partial \zeta} + \frac{\rho_{sh} \bar{\rho}}{p_{sh}} \frac{\partial v}{\partial \eta}$$
$$\times \left(-v + \frac{u_{sh} \eta}{h_1} \frac{\bar{u} \partial n_{sh}}{\partial \xi} + \frac{w \eta}{h_3} \frac{\partial n_{sh}}{\partial \zeta} \right)$$
$$+ \frac{\rho_{sh} \bar{\rho}}{p_{sh}} \left(\frac{u_{sh}^2 \bar{u}^2}{h_1} \frac{\partial h_1}{\partial \eta} + \frac{w^2}{h_3} \frac{\partial h_3}{\partial \eta} \right)$$

The normal momentum equation is first order because a second-order equation includes elliptic terms which make the equation difficult to solve. In previous studies, these equations were integrated separately to obtain v and $\bar{p}$. Srivastava et al.[6] found that this procedure had stability problems on slender bodies and suggested the use of a coupling scheme to eliminate the problem. Waskiewicz et al.[9] developed such a coupling scheme and were able to obtain solutions which approached separation on the leeside of a sphere. A similar three-dimensional coupling scheme is used in the present work.

The continuity equation is integrated from the body to the shock using a procedure similar to that of Eaton and Kaestner.[5] The shock standoff distance can then be calculated by

$$n_{sh} = \{ -(m_1)_i + [(m_1)_i^2 - 4(m_2)_i C]^{1/2} \} / 2(m_2)_i$$

where

$$m_1 = \rho_{sh} u_{sh} r \int_0^1 \bar{\rho} \bar{u} \, d\eta / \cos\theta_\phi$$

$$m_2 = \rho_{sh} u_{sh} r \kappa_\phi \cos\theta_s \int_0^1 \bar{\rho} \bar{u} \eta \, d\eta / \cos\theta_\phi$$

$$C = \tfrac{1}{2} \Delta\xi (c_i + c_{i-1}) - (m_1 n_{sh} + m_2 n_{sh}^2)_{i-1}$$

and

$$c = \rho_{sh} v_{sh} (h_1 h_3)_{\eta=1} - \rho_{sh} u_{sh} \frac{\partial n_{sh}}{\partial \xi} (h_3)_{\eta=1} - \rho_{sh} w_{sh} (h_1)_{\eta=1}$$
$$\times \frac{\partial n_{sh}}{\partial \zeta} - \frac{\rho_{sh} v_{sh} r}{\cos\theta_\phi} (\bar{\rho} \bar{v})_{\eta=0} + \int_0^1 \frac{\partial}{\partial \zeta} (n_{sh} \rho_{sh} \bar{\rho} w h_1) \, d\eta$$

Treatment of Singularities

The equations can be applied throughout a majority of the flowfield; however, there are a few points in a blunt-body flowfield where the equations become indeterminate and the limiting form must be evaluated. At the stagnation point the ξ momentum and continuity equations contain a removable singularity, and on the windward and leeward streamlines the value of $\partial w/\partial\zeta$ is needed in the continuity equation.

At a blunt stagnation point, the tangential shock velocity and the ξ derivatives of pressure and standoff distance are zero which produces a singularity in the A_3 coefficient of the ξ-momentum equation. To treat this singularity, the shock values and dependent variables are expanded in terms of ξ, as given by Anderson and Moss.[4] These expansions are substituted into the A_3 coefficient and the limit of A_3 as ξ approaches zero is used to solve the ξ-momentum equation at the stagnation point.

The singularity in the continuity equation is removed by applying the limits:

$$r\to\xi, \quad \cos\theta_s\to\xi, \quad u_{sh}\to\xi\partial u_{sh}/\partial\xi, \quad h_3\to\xi\partial h_3/\partial\xi$$

Thus, the continuity equation becomes the same as that used by Miner and Lewis[3] and can be solved by the quadratic formula for n_{sh}.

On the windward and leeward planes, the crossflow velocity is zero but the derivative with respect to ζ is nonzero. This problem is solved by taking the ζ derivative of the crossflow equation and solving for a new dependent variable w_ζ, the derivative of w. Because of the symmetry of the body, the ζ derivatives of all variables except w are zero, and the second derivative of w is zero. The equation may be written in standard parabolic form, and the coefficients of the modified ζ-momentum equation on the windward and leeward streamline are similar to those given by Eaton and Kaestner.[5]

Boundary Conditions

During re-entry at high altitudes (150,000 to 300,000 ft), low to moderate Reynolds number flows are encountered, and the low-density effects such as slip and temperature jump should be modeled.

In addition, the severe heating encountered during re-entry can cause some of the body material to ablate even at high altitudes, and this mass transfer has an effect on the flowfield. For axisymmetric flow, the coupling of wall slip and mass transfer was developed by Whitehead and Davis,[2] and the shock-slip condition is the same as that used by Davis.[1]

Wall Conditions

The slip-flow conditions with mass transfer through a porous wall, as given by Whitehead and Davis,[2] have been slightly modified. The pressure in the chamber p_l is assumed to be equal to p_w and the number density N_l is assumed to be N_w. For the case of ablation, the porosity of the wall is zero, so these assumptions will not affect the solution. The equations used in the present work are:

$$\bar{u}=\frac{\epsilon^2(2-\theta_t)}{\theta_t}\frac{5\pi}{16}\left(\frac{\pi(\gamma-1)}{2\gamma}T_{sh}\bar{T}\right)^{1/2}\frac{\mu_{sh}\bar{\mu}}{p_{sh}n_{sh}\bar{p}}\left(\frac{\partial\bar{u}}{\partial\eta}-\frac{\partial h_l}{\partial\eta}\frac{\bar{u}}{h_l}\right)$$

$$\bar{w}=\frac{\epsilon^2(2-\theta_t)}{\theta_t}\frac{5\pi}{16}\left(\frac{\pi(\gamma-1)}{2\gamma}T_{sh}\bar{T}\right)^{1/2}\frac{\mu_{sh}\bar{\mu}}{p_{sh}n_{sh}\bar{p}}\left(\frac{\partial\bar{w}}{\partial\eta}-\frac{\partial h_3}{\partial\eta}\frac{\bar{w}}{h_3}\right)$$

$$\bar{p}_w=\frac{\bar{p}-\epsilon^2\frac{15}{16}\frac{(2-\theta_t)}{\theta_t}\left(\frac{\pi(\gamma-1)}{\gamma}\frac{1}{T_{sh}\bar{T}}\right)^{1/2}\frac{\mu_{sh}T_{sh}\bar{\mu}}{p_{sh}n_{sh}}\frac{\partial\bar{T}}{\partial\eta}}{\left(1-2\sqrt{\frac{2}{\pi}}v_{sh}(\bar{v}'-\beta\bar{v}'_w)\right)}$$

$$\bar{\rho}_w=\bar{p}_w/R\bar{T}_w, \quad \bar{v}_w=(\bar{\rho}\bar{v})_w/\bar{\rho}_w, \quad v=(\bar{\rho}\bar{v})_w/\bar{\rho},$$

$$N_w=\bar{p}_w/mR\bar{T}_w$$

$$N=2(1-\beta)N_w\sqrt{\frac{\bar{T}_w}{\bar{T}}}\Big/\left[\sqrt{2\pi}v_{sh}\bar{v}'+2-\frac{\beta N_w}{N}\sqrt{\frac{\bar{T}_w}{\bar{T}}}\left(2+\sqrt{2\pi}v_{sh}\bar{v}'_w\right)\right]$$

and

$$\bar{T}=4T_w\frac{C}{A}-\frac{\epsilon^2B}{A}$$

where

$$A=8\left[\frac{1-\beta N_w}{N}\left(\frac{\bar{T}_w}{\bar{T}}\right)^{3/2}\right]+5\sqrt{2\pi}\frac{2-\alpha_t}{\alpha_t}v_{sh}\bar{v}'-\frac{\beta N_w}{N}\left(\frac{\bar{T}_w}{\bar{T}}\right)^{3/2}5\sqrt{2\pi}v_{sh}v'_w$$

$$B=\frac{2-\alpha_t}{\alpha_t}\frac{75\pi}{32}\frac{\mu_{sh}\bar{\mu}T_{sh}}{p_{sh}\bar{p}n_{sh}}\frac{\partial\bar{T}}{\partial\eta}\left(\frac{2\pi(\gamma-1)}{\gamma}T_{sh}\bar{T}\right)^{1/2}$$

$$C=2\left(1-\frac{\beta N_w}{N}\sqrt{\frac{\bar{T}_w}{\bar{T}}}\right)-\sqrt{2\pi}v_{sh}\bar{v}'-\beta\frac{N_w}{N}\left(\frac{2\pi\bar{T}_w}{\bar{T}}\right)^{1/2}v_{sh}\bar{v}'_w$$

Shock Conditions

The shock boundary conditions with slip are the modified Rankine-Hugoniot equations used by Davis.[1] The angle between the freestream velocity vector and a vector tangent to the shock surface and in the plane formed by the normal vector and the freestream velocity vector is denoted by σ. The derivation of σ is given by Rakich.[10] The equations for the conditions behind the shock are:

$$\rho_{sh}\hat{v}_{sh}=-\sin\sigma$$

$$\epsilon^2\mu_{sh}\left(\frac{\partial\hat{u}}{\partial n}\right)_{sh}+\sin\sigma\hat{u}_{sh}=\sin\sigma\cos\sigma$$

$$\frac{\epsilon^2\mu_{sh}}{Pr}\left(\frac{\partial T}{\partial n}\right)_{sh}+\sin\sigma T_{sh}-\frac{\sin\sigma}{2}(\hat{u}_{sh}-\cos\sigma)^2=\frac{\sin\sigma}{2}\left(\frac{4\gamma\sin^2\sigma}{(\gamma+1)^2}+\frac{2}{(\gamma-1)M_\infty^2}-\frac{4(\gamma-1)}{(\gamma+1)^2M_\infty^2}-\frac{4}{(\gamma+1)^2M_\infty^4\sin^2\sigma}\right)$$

$$p_{sh}=\frac{2\sin^2\sigma}{\gamma+1}-\frac{\gamma-1}{\gamma(\gamma+1)M_\infty^2}, \quad \rho_{sh}=\frac{\gamma p_{sh}}{(\gamma-1)T_{sh}}$$

The velocities must now be rotated into the body-fixed coordinate as given by Rakich.[10]

Fluid Properties

In the calculation of a flowfield solution, it will be necessary to specify certain properties of the flow. The present model assumes a perfect gas flow and allows for several property values to be specified as input data.

The ratio of specific heats γ, the gas constant R, and the Prandtl number Pr are input constants. The other gas properties are calculated from perfect gas relations.

$$c_p=\gamma R/(\gamma-1), \quad a=(\gamma RT)^{1/2}, \quad \rho=p/RT$$

The viscosity is calculated from Sutherland's viscosity law

$$\bar{\mu}=[(T_{sh}+C')/(T_{sh}\bar{T}+C')]\bar{T}^{3/2}$$

where $C'=198.6/(\gamma-1)M_\infty^2 T_\infty^*$.

The preceding relations are used to determine the thermodynamic and transport properties of the flowfield.

Method of Solution

The finite-difference method used to solve the ξ-momentum, ζ-momentum, and energy equations is the same as that used by Frieders and Lewis.[11] The equations are written in the standard form

$$A_0\frac{\partial^2 W}{\partial\eta^2}+A_1\frac{\partial W}{\partial\eta}+A_2 W+A_3+A_4\frac{\partial W}{\partial\xi}+A_5\frac{\partial W}{\partial\zeta}=0$$

The derivatives are evaluated by finite-difference expressions using the zig-zag method of Krause[12] for the cross-derivatives as follows:

$$\frac{\partial W}{\partial\zeta}=\frac{(W_{i-1,j,k+1}-W_{i-1,j,k})+(W_{i,j,k}-W_{i,j,k-1})}{2\Delta\zeta}$$

This expression is substituted into the parabolic equation, and a finite-difference form is obtained which can be solved using the Thomas algorithm.

Solution Procedure

In previous investigations, the shock-layer equations were solved using global iterations to remove the elliptic effect of the $\partial n_{sh}/\partial\xi$ and $\partial v/\partial\xi$ terms. The first iteration assumed $\partial n_{sh}/\partial\xi$ to be zero and used the thin viscous shock-layer (TVSL) approximation which eliminated the terms involving v in the normal momentum equation. Subsequent iterations used the values of $\partial n_{sh}/\partial\xi$ and v from the previous iteration. In the present method the initial estimate of $\partial n_{sh}/\partial\xi$ is obtained from an inviscid solution, and the v terms are treated with an implicit difference scheme in the normal momentum equation using a backward difference for $\partial v/\partial\xi$. The coupling of the normal momentum and continuity equations[9] has eliminated the stability problems which occurred in the earlier procedure and permits one to solve the fully viscous shock-layer (FVSL) equations without requiring the v profiles from the previous global iteration. This procedure eliminates the need for global iteration provided the inviscid shock shape is suitably accurate.

The solution begins on the spherically blunted nose by obtaining an axisymmetric solution in the wind-fixed coordinate system where $\xi=0$ at the stagnation point. At a specified location (usually the sphere-cone tangent point), the axisymmetric solution is rotated into a body-fixed coordinate system where $\xi=0$ at the geometric nosetip of the vehicle. The tangential velocity is resolved into two components u and w using the method described by Waskiewicz and Lewis,[13] and these rotated profiles are used as initial data for the three-dimensional solution. The three-dimensional solution begins on the windward plane and marches around the body obtaining a converged solution at each ζ step. After completing a sweep in ζ, the procedure then steps downstream in ξ along the windward streamline and begins the next ζ sweep. At each point the equations are solved in the following order: 1) ζ momentum, 2) energy, 3) ξ momentum, 4) integration of continuity for n_{sh}, and 5) the coupled continuity and normal momentum equations.

A discontinuity in the body curvature κ exists at the sphere-cone tangent point. To avoid the adverse effects of this discontinuity, the procedure is not permitted to difference across the juncture. Since the present method uses a two-point backward difference for the streamwise derivatives, all problems with the discontinuity in κ are avoided by simply requiring a solution at the sphere-cone tangent point.

Surface Quantities

The surface conditions in two-dimensional flows with wall slip and mass transfer are given by Whitehead and Davis.[14] The anlaysis is extended to three dimensions in Ref. 8, and the resulting skin-friction and heat-transfer coefficients are:

$$C_{f_\xi}=\frac{2\epsilon^2\mu_{sh}u_{sh}\bar{\mu}}{n_{sh}}\left(\frac{h_1\partial\bar{u}}{\partial\eta}-\frac{\bar{u}\partial h_1}{\partial\eta}\right)-2\rho_{sh}v_{sh}u_{sh}\bar{\rho}_w\bar{v}_w\bar{u}$$

$$C_{f_\zeta}=\frac{2\epsilon^2\mu_{sh}w_{sh}\bar{\mu}}{n_{sh}}\left(\frac{\partial\bar{w}}{\partial\eta}-\frac{\partial h_3}{\partial\eta}\frac{\bar{w}}{h_3}\right)-2\rho_{sh}v_{sh}w_{sh}\bar{\rho}_w\bar{v}_w\bar{w}$$

$$q_w=-\frac{\epsilon^2\mu_{sh}T_{sh}\bar{\mu}}{Prn_{sh}}\frac{\partial\bar{T}}{\partial\eta}-\frac{\epsilon^2\mu_{sh}u_{sh}^2\bar{u}}{n_{sh}}\left(\frac{\partial\bar{u}}{\partial\eta}-\frac{\bar{u}\partial h_1}{\partial\eta}\right)\bar{\mu}$$

$$-\bar{\mu}\bar{w}\frac{\epsilon^2\mu_{sh}w_{sh}^2}{n_{sh}}\left(\frac{\partial\bar{w}}{\partial\eta}-\frac{\bar{w}}{h_3}\frac{\partial h_3}{\partial\eta}\right)+\rho_{sh}T_{sh}\bar{\rho}_w v_w(\bar{T}-\bar{T}_w)/\gamma$$

$$-p_{sh}v_{sh}\bar{\rho}(\bar{v}_w-v)+\frac{3\rho_{sh}v_{sh}\bar{\rho}_w\bar{v}_w}{2}[(u_{sh}\bar{u})^2+(w_{sh}\bar{w})^2]$$

$$St_\infty=-q_w^*/\rho_\infty U_\infty(H_0^*-H_w^*)$$

Results and Discussion

Three cases were selected to validate the three-dimensional viscous shock-layer (VSL3D) code and test its limitations. The first case was for conditions of a wind-tunnel test on a 10-deg half-angle sphere-cone at $\alpha=10$ deg and $M_\infty=18$. Boylan[15] and Kinslow[16] measured heat-transfer and pressure distributions on this body. The second case was a drag test on a short sphere-cone at $M_\infty=10.17$ by Boylan and Sims.[17] The third case was a 7-deg half-angle sphere-cone at 38-deg angle of attack at $M_\infty=25.81$. A parabolized Navier-Stokes (PNS) solution was used for comparison with this case. The conditions for all test cases are summarized in Table 1.

Figure 2 compares the heat-transfer data of Boylan with the predictions of the VSL3D and PNS codes. The agreement on the windward streamline was quite good but became poorer on the leeward side. The VSL3D solution agreed well with the PNS prediction. The effect of slip decreased with heat transfer on the windward side and improved the agreement of the VSL3D prediction with the experimental data.

Table 1 Test case conditions

Case	Alt, ft (km)	U_∞, ft/s (m/s)	M_∞	T_∞, °R (K)	α, deg	θ_c, deg	$Re_\infty\times10^{-4}$, ft^{-1} (m^{-1})	T_w/T_0	ϵ
1	Wind tunnel	7941 (2420)	18.0	81 (45)	10	10	1.583 (5.194)	0.11	0.287
2	Wind tunnel	6534 (1992)	10.17	171.8 (95.44)	0-40	10	1.139 (3.737)	0.25	0.259
3	240,000 (73.2)	24472 (7459)	25.81	374.15 (207.9)	38	7	0.938 (3.077)	0.012	0.133

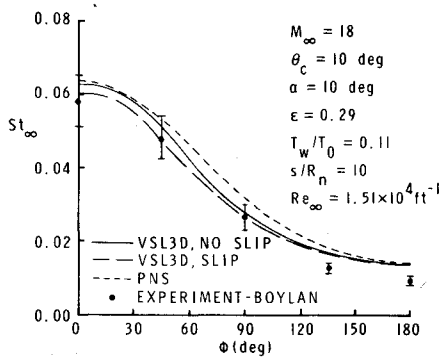

Fig. 2 Predicted heat-transfer distribution around a 10-deg sphere-cone compared with the experimental data of Boylan at $s/R_n = 10$.

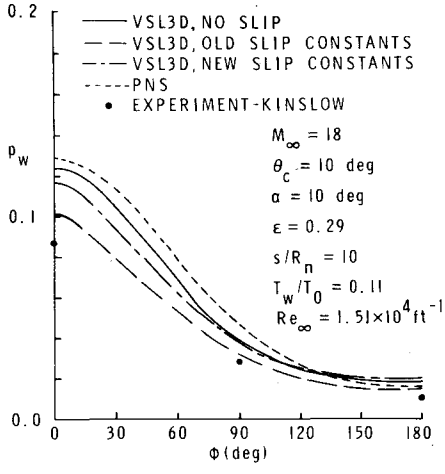

Fig. 3 Wall pressure distribution around a 10-deg sphere-cone compared with the experimental data of Kinslow at $s/R_n = 10$.

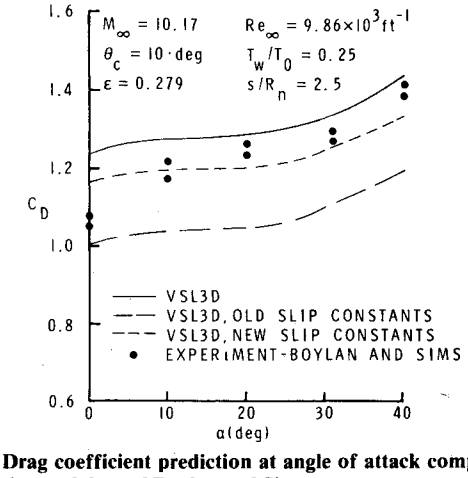

Fig. 4 Drag coefficient prediction at angle of attack compared with the experimental data of Boylan and Sims.

Comparisons with the Kinslow data for the same conditions are made in Fig. 3. Two different sets of slip constants are used in these calculations. The first set is the classical slip constants derived by Whitehead and Davis,[14] and the second set is the modified slip constants used by Srivastava et al.[18] to correct the underprediction of the stagnation point pressure. Figure 3 presents the circumferential pressure distribution at $s = 10$. The VSL3D and PNS predictions were high on the windward streamline but were reduced considerably when the slip conditions were used. The classical slip constants gave much better predictions of the wall pressure than the modified constants.

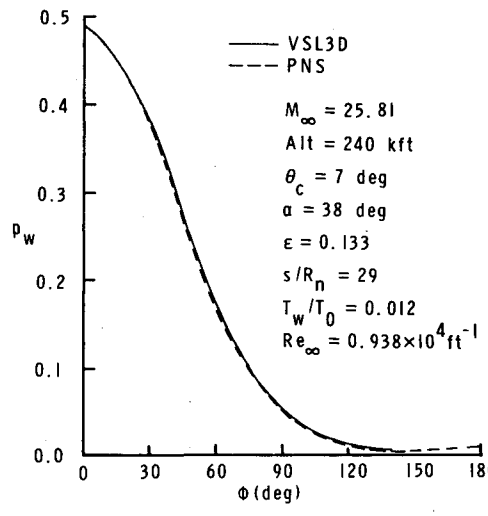

Fig. 5 Wall pressure prediction around a sphere-cone at 38-deg angle of attack.

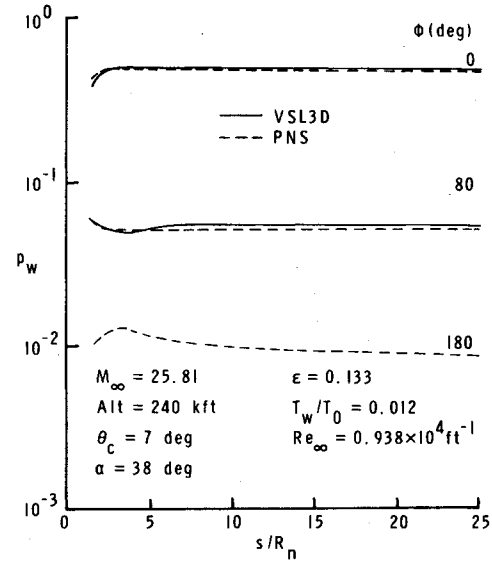

Fig. 6 Wall pressure distribution along a sphere-cone at 38-deg angle of attack.

The experimental data available from Boylan and Sims[17] were the drag coefficients at angles of attack from $\alpha = 0$-40 deg. Figure 4 compares the experimental data with shock-layer solutions without slip and with the two sets of slip constants. The solution without slip was high as expected, and the effect of slip reduced the drag coefficient. The modified slip constants gave a better prediction for this case than the prediction using the classical slip constants. Srivastava et al.[18] modified the constants to increase the pressure at the stagnation point. For the conditions of Boylan and Sims, the modified constants gave better predictions, but at the conditions of Kinslow, the classical constants gave better agreement. This may be caused by the shorter body used by Boylan and Sims which is more sensitive to the spherical nose solution. It is impossible to accurately evaluate the two sets of slip constants from these two cases since the results are conflicting. The modified constants give better predictions in the nose region, but downstream the predictions using the classical constants seem to be in better agreement. More experimental data are needed to evaluate the modified slip constants.

Case 3 is a free-flight case corresponding to an altitude of 240 kft. This case has a significant crossflow separation region because of the high angle of attack and the long body.

Table 2 Computation times[a]

Case	α, deg	Slip	Number of grid points ξ	η	ζ	VSL3D Total time, h:min:s	VSL3D Time/ step, min.	PNS Total time, h:min:s	PNS Time/ step, min.
1	10	No	46	61	10	32:30	0.706	—	—
	10	No	81	101	19	—	—	4:43:34	2.948
	10	Yes	32	61	10	60:13	1.875	—	—
2	30	No	6	61	10	7.33	1.25	No solution	
	30	Yes	6	101	10	17:25	2.90	No solution	
3	38	No	75	61	7/10[b]	44:03	0.587	—	—
	38	No	76	101	19	—	—	6:43:03	4.287

[a] IBM 370/158 FORTRAN H, OPT = 2. [b] Planes were dropped due to crossflow separation. The number tabulated, e.g., 8/10, gives the average number of planes per ξ step, 8 with a maximum of 10 planes down to crossflow separation.

The cones used by Boylan and Sims were so short that the crossflow did not separate, even though the angle of attack was 40 deg. Experimental data were not available for comparison, but the PNS solutions obtained by Waskiewicz and Lewis[19] were used to check the validity of the VSL3D solution. The parabolic treatment of the crossflow momentum equation prevented solutions from being obtained on the leeward side using the present method. When crossflow separation occurred, the solution stopped marching around the body but continued marching downstream. The ζ derivatives on the last ζ plane were changed to backward derivatives instead of the zig-zag derivatives used elsewhere. The inconsistencies between the two derivative evaluations cause some problems with the solution at the last plane, especially in the calculation of the standoff distance. Figures 5 and 6 compare the wall pressure distributions with a PNS solution. The agreement between the VSL3D and PNS solutions is good until the VSL3D code begins to drop ζ planes at $s = 7$. Afterwards the pressure on the 80-deg plane becomes high. The circumferential distribution shows the wall pressure at $s = 29$. The shock-layer prediction is in good agreement on the windward planes but becomes higher as the solution sweeps around the body. The shock shape predictions are shown in Fig. 7 and compared with the PNS solution. The prediction on the windward planes is good even at this large angle of attack.

These test cases have been used in an attempt to validate the VSL3D code. Comparisons have shown that the shock layer gives good predictions of the entire flowfield at lower angles of attack. The VSL3D predictions were actually in better agreement with the experimental data than the PNS solutions for the Boylan[15] and Kinslow[16] conditions, and the ability to use the slip boundary conditions improved the VSL3D prediction. At high angles of attack, the VSL3D technique could be used to make reasonably accurate predictions on the windward side planes, but the parabolic treatment of the crossflow momentum equation prevents a solution in the separated region.

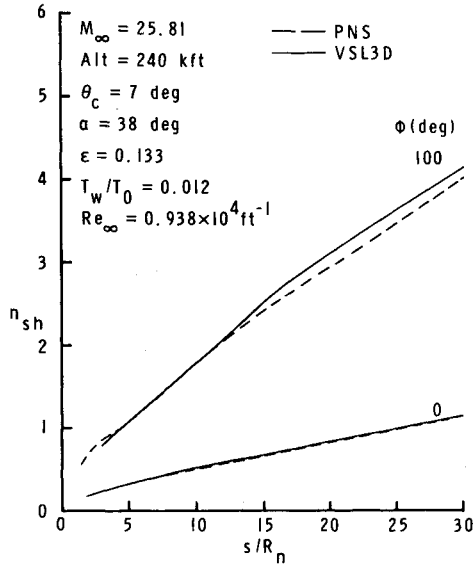

Fig. 7 Shock-shape distribution along a sphere-cone at 38-deg angle of attack.

The shock-layer approach must also be efficient in computing cost to be a useful tool. Even though the predictions are good, the computing time required must be reasonable or the cost of obtaining a solution may be prohibitive for use as an engineering tool. Table 2 presents a summary of the computing times required for these calculations and compares the present VSL3D method with the times required for a parabolized Navier-Stokes solution. The typical solution time for the VSL3D is 4 to 8 times faster than the PNS solution, and this factor could be increased by allowing the VSL3D solution to take longer step sizes downstream. The solution procedure for the PNS code has a limit on the step size in the streamwise direction (see Lubard and Helliwell[7] and Waskiewicz and Lewis[19]). The shock-layer equations, being parabolic in both directions, should not have such a maximum step size. When the slip effects were being considered, there was a substantial increase in computing time because the boundary conditions were no longer fixed, but must also be iterated to obtain a converged solution. When using slip at the larger angles of attack, it is sometimes necessary to increase the number of points in the normal direction to obtain reasonably accurate derivatives near the wall and shock. Of course, this slows the solution down even more as indicated in the computing times for case 2. Finally, note that the time per step was more for case 2 without slip than for case 1. This is because the sphere-cone in case 2 was shorter than in case 1. Near the sphere-cone tangent point, the solution required more iterations than down on the conical afterbody, and on the short cone this increase caused a larger average computing time per ξ step. Thus, the viscous shock-layer approach gives reasonably accurate predictions and is much more efficient than the PNS technique, at least up to crossflow separation. Such advantages make the VSL3D code a useful tool in engineering analysis and design.

Conclusions

The viscous shock-layer equations have been extended to complete three-dimensional blunt-nosed bodies at high angles of attack. Comparison with experimental data show that the shock-layer technique may be used to obtain good predictions of the complete flowfield on sphere-cones at low angles of attack, i.e., $\alpha = 10$ deg or on short cones where the crossflow velocity does not separate. On long cones at large angles of attack, the parabolic treatment of the crossflow momentum equations prevents solutions on the leeward side beyond crossflow separation. More work is needed to improve the quality of the solution near the separated region and allow the

code to march further around the body. Comparison with the PNS solutions show that VSL3D gives reasonably accurate predictions on the windward side even at high angles of attack. Finally, the computing time for the VSL3D solution is between 4 and 8 times faster than the PNS approach for the same flow conditions and could be even faster if larger step sizes were used on the conical portion of the body.

References

[1]Davis, R. T., "Numerical Solution of the Hypersonic Viscous Shock Layer Equations," *AIAA Journal*, Vol. 8, May 1970, pp. 843-851.

[2]Whitehead, R. E. and Davis, R. T., "Numerical Solutions to the Viscous Shock-Layer Blunt Body Problem with Inert Gas Injection," Sandia Laboratories, SC-CR-70-6162, Jan. 1971.

[3]Miner, E. W. and Lewis, C. H., "Hypersonic Ionizing Air Viscous Shock Layer Flows over Nonanalytic Blunt Bodies," NASA CR-2550, May 1975.

[4]Anderson, E. C. and Moss, J. N., "Numerical Solution of the Hypersonic Viscous-Shock Layer Equations for Laminar, Transitional and Turbulent Flows of a Perfect Gas over Blunt Axially Symmetric Bodies," NASA TN D-7865, Feb. 1975.

[5]Eaton, R. R. and Kaestner, P. C., "Viscous Shock-Layer Flow in the Windward Plane of Cones at Angles of Attack," Sandia Laboratories, SC-RR-72-0449, March 1973.

[6]Srivastava, B. N., Werle, M. J., and Davis, R. T., "Viscous Shock-Layer Solutions for Hypersonic Sphere-Cones," AIAA Paper 77-693, June 1977.

[7]Lubard, S. C., and Helliwell, W. S., "Calculation of the Flow on a Cone at High Angle of Attack," *AIAA Journal*, Vol. 12, July 1974, pp. 965-974.

[8]Murray, A. L. and Lewis, C. H., "Three-Dimensional Fully Viscous Shock-Layer Flows over Sphere-Cones at High Altitudes and High Angles of Attack," VPI&SU-AERO-078, Jan. 1978.

[9]Waskiewicz, J. D., Murray, A. L., and Lewis, C. H., "Hypersonic Viscous Shock Layer Flow over a Highly Cooled Sphere," *AIAA Journal*, Vol. 16, Feb. 1978, pp. 189-192.

[10]Rakich, J. V., "A Method of Characteristics for Steady 3-D Supersonic Flow with Application to Inclined Bodies of Revolution," NASA TN D-5341, Oct. 1969.

[11]Frieders, M. C. and Lewis, C. H., "Effects of Mass Transfer into Laminar and Turbulent Boundary Layers over Cones at Angles of Attack," VPI-AERO-031, March 1975.

[12]Krause, E., "Comment on 'Solution of a Three-Dimensional Boundary-Layer Flow with Separation'," *AIAA Journal*, Vol. 7, March 1969, pp. 575-576.

[13]Waskiewicz, J. D. and Lewis, C. H., "Recent Developments in Viscous Shock-Layer Theory," VPI&SU-AERO-079, March 1978.

[14]Whitehead, R. E. and Davis, R. T., "Surface Conditions in Slip-Flow with Mass Transfer," VPI-E-59-11, Dec. 1969.

[15]Boylan, D. E., "Laminar Heat Transfer on Sharp and Blunt Ten-Degree Cones in Conical and Parallel Low-Density Flow," AEDC-TR-106, Aug. 1973.

[16]Kinslow, M., "Static Pressure on Sharp and Blunt Cones in Conical and Parallel Low-Density Flow," AEDC-TR-74-30, Nov. 1974.

[17]Boylan, D. E. and Sims, W. H., "Experimental Determination of Aerodynamic Drag on a Blunted 10-Deg Cone at Angles of Attack in Hypersonic, Rarefied Flow," AEDC-TR-64-60, April 1964.

[18]Srivastava, B. N., Davis, R. T., and Werle, M. J., "Slip Model for Hypersonic Viscous Flow," *AIAA Journal*, Vol. 14, Feb. 1976, pp. 257-259.

[19]Waskiewicz, J. D. and Lewis, C. H., "Hypersonic Viscous Flows over Sphere Cones at Angles of Attack," AIAA Paper 78-64, Jan. 1978.